A nonlinear dynamic model of the vibration response of defective rolling element bearings

Alireza Moazenahmadi, Dick Petersen and Carl Howard

School of Mechanical Engineering, The University of Adelaide, South Australia, Australia

ABSTRACT

This paper presents a nonlinear dynamic model of the contact forces and vibration generated in rolling element bearings due to a surface defect in a raceway. A rectangular shape defect with sharp edges is selected for modelling because previous models were not able to predict the low frequency vibration event that occurs when a rolling element enters the defect. Simulations are presented for two defect sizes. In the first simulation, the defect length is small such that the rolling elements do not strike the bottom of the defect. The simulated results compare well with experimental results, and predict the low and high frequency events that occur when a rolling element passes through the defect observed in the experimental results. In the second simulation, the defect length is increased such that a rolling element strikes the bottom of the defect. This simulation demonstrates the benefits over models that do not consider the mass of the rolling elements. The benefits are illustrated by a detailed analysis of the contact forces that occur as a rolling element passes through the defect. The developed model can be used to simulate the vibration response of bearings with a defect in the raceway to aid in the development of new diagnostic algorithms.

INTRODUCTION

Rolling element bearings are widely used in rotary machinery. Developing an understanding of their dynamic behaviour has therefore received a great deal of attention and led to the development of a number of analytical models. These models are often used to develop and test diagnostic algorithms for condition monitoring purposes.

This paper develops a dynamic model that can be used to predict the contact forces and vibration response of a wide range of defect profiles. However, this paper focuses on rectangular shaped bearing defects with sharp edges. The non-linear model includes the dynamics of the raceways and rolling elements, the mass and the inertia of rolling elements and the impact energy loss of the rolling elements in the system. The model can be used to predict the vibration and contact forces of parts of the bearing, and does not require an assumed path of a rolling element moving into and out of a defect. The model is based on the work by Harsha (2005).

The model described in this paper is compared with experimental studies by Sawalhi and Randall (2011). The size of the defects in their experimental study was small, compared to the rolling element diameter, and the rolling elements did not strike the bottom of the defect.

A second case study is described in this paper of a simulation involving a larger defect, where the rolling element loses contact with both raceways and can strike the bottom of the defect in the raceway. The characteristics of the resultant vibration signal for both case studies are discussed. This model can be used to simulate the vibration signal generated by bearings for several types of defects, and can be used to develop new diagnostic algorithms including algorithms to identify the size of a defect.

Previous work

Numerous vibration generation mechanisms in rolling element bearings have been investigated by researchers. These mechanisms include varying compliance due to the existence of different rolling elements in the load zone, localised defects such as cracks, pits and spalls caused by fatigue, and distributed defects such as waviness due to manufacturing errors (Sunnersjö, 1978, Sayles and Poon, 1981, Wardle, 1988, Tandon and Choudhury, 1999, Jang and Jeong, 2004). The study of the vibration generated by the above mentioned mechanisms is useful for quality inspection and condition monitoring.

A force impulse train is often used to model the vibration response of a defective bearing (Sunnersjö, 1978, Jang and Jeong, 2004). The impulse train models have received considerable attention for developing condition monitoring algorithms. These models do not take the shape and size of a localised fault into account and are limited to bearing defects that produce impulsive vibration signals. Hence, this simple model cannot be employed to analyse the vibration response of defects of varying shape and size.

Recently, more sophisticated dynamic models have been developed to include defect geometries that are distributed or localised. In these models, the bearing contact forces are related to the displacement of bearing components using Hertzian contact theory (Harsha et al., 2003, Sawalhi and Randall, 2008). The mass and inertia of the rolling elements in these models can safely be ignored for low speed applications because the centrifugal forces or gyroscopic moments in most rolling element bearing applications are much smaller than the contact forces between the rolling elements and raceways due to the external radial and/or axial loads (Liew et al., 2002). These forces do not significantly affect the distribution of the applied load among the rolling elements and are usually ignored in dynamic analysis of rolling element bearings. Due to this simplification in the earlier models, the force impacts that are generated as unloaded rolling elements strike the bottom of the defect cannot be predicted.

A more complex model was developed by Harsha (2005) which includes the mass and the inertia of the rolling elements. However, the impact energy loss of the rolling elements was not taken into account and therefore impact forces of the rolling elements striking the raceways cannot be predicted. In addition, the model develop by Harsha (2005) does

not include a mass-spring-damper representing a measured high frequency resonant response of the bearing, as included in the model proposed by Sawalhi & Randall (2008).

Figure 1 shows a typical measured vibration signal due to a defect with sharp edges, such as illustrated in the outer raceway in Figure 2. A limitation of all previously mentioned models is that simulations of a defect with sharp edges produces very large impulsive forces at both the entrance and exit of the defect, which results in large accelerations with high frequency content. In contrast, it has been shown by previous experimental studies that the entry of a rolling element to a defect with a sharp edge produces a vibration signal with low frequency content (Epps and Mccallion, Sawalhi and Randall, 2011). The exit of the rolling element produces a larger vibration signal with high frequency content, which is due to the rolling element striking the sharp edged raceway and exciting the natural frequency of the system.
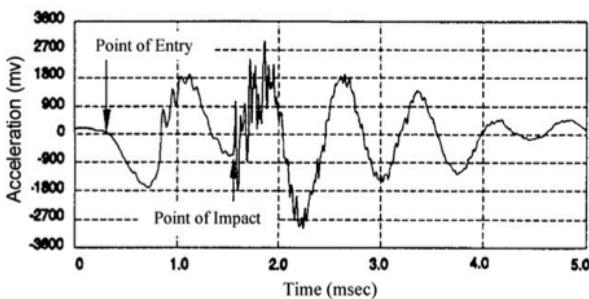

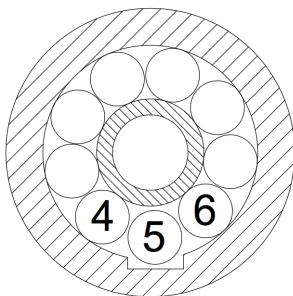Figure 1: A typical measured response (Epps and Mccallion)

Figure 2. Schematic diagram of the second simulated bearing with square shape defect (a defect with sharp edges).

In order to avoid large impulsive forces at the entrance and exit points of a square shape defect, Sawalhi and Randall (2008) modified the shape of the defect to resemble the path travelled by the rolling element. In the model developed here, the path of the rolling element is predicted taking into account its mass and finite dimension, and the actual defect geometry is therefore used as a model input.

The following sections describe a proposed model that overcomes some of the limitations of previous models.

MODELING AND PROBLEM FORMULATION

Figure 3 shows the main components of a rolling element bearing, namely the inner raceway, the outer raceway and the rolling elements. The rolling element bearing assembly is modelled as a multi-body dynamic system consisting of masses, springs and dampers, with the assumption that the outer raceway is fixed. Compared to Harsha's (2005) model, an additional mass m has been attached to the inner raceway via a spring and damper to account for the high frequency resonant response of the bearing.
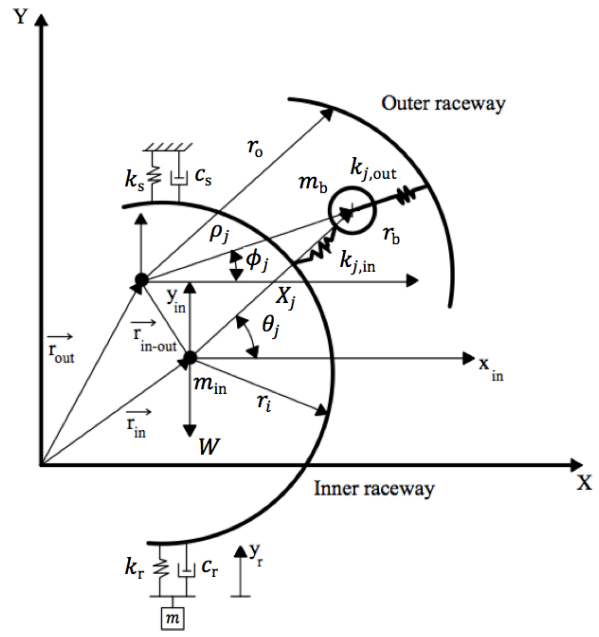
Symbol	Description
r_o	Radius of outer raceway
r_b	Radius of rolling element
r_i	Radius of inner raceway
ρ_j	Radial position of the rolling element from the centre of the outer raceway
X_j	Radial position of the rolling element from the centre of the inner raceway
ϕ_j	Angular position of jth rolling element with respect to centre of the outer raceway
θ_j	Angular position of jth rolling element with respect to centre of the inner raceway
$k_{j,out}$	Contact stiffness between the inner raceway and j^{th} rolling element
$k_{j,in}$	Contact stiffness between the inner raceway and j^{th} rolling element
c_s	Damping of the shaft
k_s	Stiffness of the shaft
c_r	Damping of high frequency resonant mode
k_r	Stiffness of high frequency resonant mode
m	Mass of high frequency resonant mode
N_b	Number of rolling elements
m_b	Mass of the jth rolling element
m_{in}	Mass of the inner ring
W	Static load acting on the inner raceway

Figure 3. The diagram of a spring-mass model for rolling element bearings

A set of independents generalised coordinates for the inner raceway (x_{in}, y_{in}), and the rolling elements (ρ_j ; j=1, 2, 3,…, N_{b}) are defined. The parameter X_j is the position of the jth rolling element from the centre of the inner raceway and is related to the parameter ρ_j as

$$X_j = \left[x_{\text{in}}{}^2 + \rho_j{}^2 - 2\rho_j x_{\text{in}} \cos \phi_j \right. \\ \left. - 2\rho_j y_{\text{in}} \sin \phi_j + y_{\text{in}}\right]^{1/2} \qquad (1)$$

where ϕ_j is the angular position of the jth rolling element with respect to the inner raceway's generalised coordinate illustrated in Figure 3. Non-linear springs are used to model the contacts between the rolling elements and raceways. The contact forces are related to the elastic contact deformations between the rolling elements and raceways using the Hertzian elastic contact theory (Stachowiak and Batchelor, 2011). The contact deformations of a rolling element and the raceways are calculated from the dynamic motion of the bearing components. Therefore the nonlinear contact stiffnesses are related to the dynamics of the system.

Contact stiffness

The contact deformations and forces between the rolling elements and the raceways are modelled using Hertzian contact theory (Stachowiak and Batchelor, 2011). The contact force Q_j between a rolling element and raceway is calculated as

$$Q_j = k_j(\delta_j)\delta_j \qquad (2)$$

where the nonlinear contact stiffness $k_j(\delta_j)$, which is a function of the contact deformation δ_j, is defined for a steel-ball and steel raceway contact as

$$k_j(\delta_j) = k_c \, \delta_j{}^{1/2} \qquad (3)$$

with the constant k_c depending on the curvature of the rolling elements and raceways (Harris, 2001). Equation (3) is used for calculating the nonlinear stiffnesses of the springs $k_{j,\text{in}}$ and $k_{j,\text{out}}$ shown in Figure 3, given the contact deformations $\delta_{j,\text{in}}$ and $\delta_{j,\text{out}}$ between the jth ball and inner and outer raceway, respectively. Equations (3) has to be adjusted when rollers are used instead of balls (Harris, 2001).

Modelling the defect and contact deformations

In order to model the geometry of a defect on the raceways, the defect shape function γ is introduced, which is a function of the angle ϕ_j. A rectangular-shape bearing defect on the outer raceway can be modelled as

$$\gamma(\phi) = \begin{cases} \Delta & \phi_{\text{en}} < \phi < \phi_{\text{ex}} \\ 0 & \text{otherwise} \end{cases} \qquad (4)$$

where ϕ_{en} and ϕ_{ex} are the angular positions of the entry and the exit to the defect, respectively.

In contrast to the previous models (Harsha, 2005, Sawalhi and Randall, 2008), where the rolling element is considered as a point mass to calculate the contact deformation between each rolling element and the raceway at a time, the model proposed in this paper takes into account a finite number of points on the circumference of a rolling element for calculations. In other words, the dimensions of the rolling element are taking into account rather than modelling it as point mass.

Figure 4 shows a diagram of a rolling element in the defect zone. As a rolling element at a given angular position ϕ_j contacts the edges of the defect, the deformation δ_j occurs at the angle β_j illustrated in Figure 4.
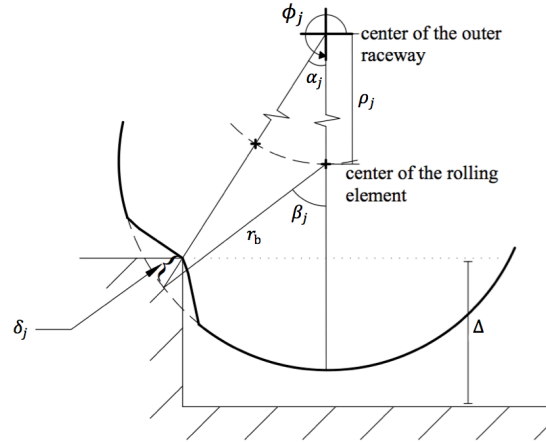

Figure 4. Schematic diagram of the rolling element passing a rectangular shape defect with δ_j the contact deformation, Δ the defect depth, r_{b} the rolling element radius, ρ_j the position of the rolling element with respect to the centre of the outer raceway, β_j the angle of the deformation location on the rolling element, and α_j the angle between the edges of the defect and the vector ρ_j.

In this paper the defect is modelled on the outer raceway. The deformations between the rolling elements and the inner raceway always happen at a point perpendicular to the inner raceway. However, the deformation between a rolling element and the outer raceway in the defect zone happens at a point which is not necessarily at the angular position $\beta_j = 0$ as assumed in previous models (Harsha, 2005). To overcome this limitation, a finite number of points on each rolling element are used to calculate the angular position of the contact deformation between a rolling element and the defect on the outer raceway. The relative contact deformations between the rolling elements and the raceways at this point are calculated as

$$\delta_{j,\text{out}} = \left[c - \gamma(\phi_j \pm \alpha_j) - r_{\text{o}} + \frac{r_{\text{b}}\sin \beta_j}{\sin \alpha_j}\right] \cos \alpha_j \qquad (5)$$

$$\delta_{j,\text{in}} = c + r_{\text{b}} + r_{\text{i}} - X_j \qquad (6)$$

where r_{b} is the rolling element radius, r_{o} is the radius of the outer raceway, r_{i} is the radius of the inner raceway, c is the radial clearance, X_j was defined in Equation (1), and the angle α_j is given by

$$\alpha_j = \tan^{-1}\left(\frac{r_{\text{b}}\sin \beta_j}{\rho_j + \cos \beta_j}\right); \ -\frac{\pi}{2} < \beta_j < \frac{\pi}{2} \qquad (7)$$

The angle α_j, illustrated in Figure 4, is the angle between the deformation point on a rolling element and the generalised coordinate ρ_j of the rolling element. These enhancements to the previous models improve the results in dynamic simulation of bearings with sharp defects by permitting the rolling element to follow a more realistic path that is not predefined.

Equations of motion

The equations of motion for the inner race, including the high frequency response of the inner race, are given by

$$m_{\text{in}}\ddot{x}_{\text{in}} - \sum_{j=1}^{N_b} k_{j,\text{in}} \left[\delta_{j,\text{out}}\right]_+ \cos\phi_j = 0 \qquad (8)$$

$$m_{\text{in}}(\ddot{y}_{\text{in}} + g) + (c_s + c_r)\dot{y}_{\text{in}} + (k_r + k_s)y_{\text{in}} - k_r y_r \qquad (9)$$
$$- c_r \dot{y}_r - \sum_{j=1}^{N_b} k_{j,\text{in}} \left[\delta_{j,\text{out}}\right]_+ \sin\phi_j$$
$$= W$$

$$m_r \ddot{y}_r + k_r(y_r - y_{\text{in}}) + c_r(\dot{y}_r - \dot{y}_{\text{in}}) = 0 \qquad (10)$$

where $g = 9.81\,\text{m/s}^2$ is the gravity of earth, W is static load applied to the shaft in the y direction, and the remaining spring and damper constants are defined in Figure 3.

In order to derive the equations of motion for the rolling elements, Lagrange's equation for the set of generalised coordinates, ρ_j are used as

$$\frac{d}{dt}\frac{\partial T}{\partial\{\dot{\rho}_j\}} - \frac{\partial T}{\partial\{\rho_j\}} + \frac{\partial V}{\partial\{\rho_j\}} = \{f\} \qquad (11)$$

where T is the kinetic energy, V is the potential energy, ρ_j is a vector with the generalised coordinates for the rolling elements, and $\{f\}$ is the vector with generalised contact forces. The total kinetic and potential energy of each rolling element is

$$T_j = \sum_{j=1}^{N_b} 0.5 m_b \left(\dot{\rho}_j{}^2 + \rho_j{}^2 \dot{\phi}_j{}^2\right) \qquad (12)$$
$$+ 0.5\, I\, \dot{\phi}_j{}^2 \left(1 + {r_o}/{r_b}\right)^2$$

$$V_j = \sum_{j=1}^{N_b} m_b g\, \rho_j \sin\phi_j \qquad (13)$$

where I is the moment of inertia of a rolling element, m_b is the rolling element mass, and r_o is the outer raceway radius. The vector of the generalised contact forces $\{f\}$ in Equation (11) acting on each rolling element can be calculated by differentiating Hooke's law for the nonlinear springs with respect to the generalised coordinates ρ_j, such that

$$\{f\} = \frac{\partial(V)_{\text{springs}}}{\partial\{\rho_j\}} \qquad (14)$$

where the potential energy of the nonlinear springs acting on each rolling element is given, according to the Hooke's law, by

$$(V_j)_{\text{springs}} = \sum_{j=1}^{N_b} 0.5\, k_{j,\text{in}} \delta_{j,\text{in}}^2 + \sum_{j=1}^{N_b} 0.5\, k_{j,\text{out}}\, \delta_{j,\text{out}}^2 \qquad (15)$$

Substituting Equations (12) to (14) into Equation (11) gives the following equations of motion for the rolling elements

$$m_b \ddot{\rho}_j + [c_{\text{rol}}]_* \dot{\rho}_j + m_j g \sin\phi_j + m_j \rho_j \dot{\phi}^2$$
$$+ k_{j,\text{in}}[\delta_{j,\text{in}}]_+ \frac{\partial\delta_{j,\text{in}}}{\partial\rho_j}$$
$$+ k_{j,\text{out}}[\delta_{j,\text{out}}]_+ + \frac{1}{2}\frac{\partial k_{j,\text{in}}}{\partial\rho_j}[\delta_{j,\text{in}}]_+^2 \qquad (16)$$
$$+ \frac{1}{2}\frac{\partial k_{j,\text{out}}}{\partial\rho_j}[\delta_{j,\text{out}}]_+^2 = 0$$

$$j = 1,2,\dots,N_b$$

where differentiation of $k_{j,\text{in}}, k_{j,\text{out}}$ and $\delta_{j,\text{in}}$ with respect to ρ_j can be obtained from Equations (3), (5) and (6), and with the function of the damper term c_{rol} described in the following. The subscript $+$ indicates that only positive values are used in the equations and the negative vales are set to zero. Thus, the contact forces only arise if a rolling element is under compression.

In Equation (16), the viscous damping parameter c_{rol} accounts for the impact energy loss of the rolling elements. The coefficient of restitution during impacts in the system can be interpreted as damping in the vibro-impact dynamics of a system (Liew et al., 2002). Therefore the loss of energy due to a rolling element impact is taken into account by including the damping c_{rol} in Equation (16). The subscript $*$ in this equation indicates that when a rolling element is not in contact with a raceway, the damping c_{rol} for that rolling element is set to zero. This is the case when a rolling element loses contact with both raceways. While the collision of a rolling element and a raceway is occurring this parameter has positive value. It is assumed that the effect of the elasto-hydrodynamic lubrication (EHL) on the rolling elements damping is small and ignorable (Wijnant et al., 1999). This addition to Harsha's model (2005) enables the prediction of the impact forces when an unloaded rolling element strikes the bottom of a defect.

Equations (8) to (10) and (16) form a system of coupled second order nonlinear ordinary differential equations having parametric excitation.

SIMULATION AND VALIDATION

To enable comparison of simulated and experimental results and validate the model, the geometrical bearing parameters are set similar to the bearing in the experimental test bearing used by Sawalhi and Randall (2011). The test bearing used in this experiment was a deep grove ball on which a rectangular shape outer raceway defect with a width of 1.1 mm and a depth of 0.25 mm was machined. The bearing has a pitch diameter of 39 mm and a rolling element diameter of 7.93 mm. The vibration measurements were recorded at a rotational speed of 1200 rpm. The high frequency resonant mode was modelled to have a resonance frequency of 30 kHz and a damping ratio of 8%. The simulations were undertaken using Matlab® and Simulink® and the equations of motion defined by Equations (8) to (10) and (16) were solved using the 'ode45' differential equation solver.

The aim of the simulations is to show that the developed model can predict characteristics observed in a measured vibration response (Sawalhi and Randall, 2011) while modelling the actual shape of the defect. This is in contrast to previous models in which the modelled defect shape was altered

from the actual shape in order to achieve better agreement between modelled and measured results. The emphasis here is on predicting the qualitative characteristics of the vibration signal rather than fine tuning the damping and stiffness terms of the model to obtain absolute vibration levels that match the measured ones.

The advantages of the developed model are demonstrated by showing that: (1) It can predict the low and high frequency content of the vibration signal due to the rolling element passing a rectangular shape defect with sharp edges similar to the experimental result; (2) The relative position of the two frequency components on the simulated vibration signal matches experimental results. The developed model is also used to analyse the contact forces between the rolling elements and raceways.

Figure 5(a) shows the trace of the radial position of the 5th rolling element ($\rho_j + r_b$). The entry to the defect appears with mainly low frequency content while the exit from the defect has higher frequency content. The low frequency content at the entry to the defect is due to gradual de-stressing of the rolling element which starts when it is at an angle ϕ_{en}. This gradual de-stressing is observed in Figure 5(c) where the contact forces gradually decay until the rolling element changes direction and moves out of the defect. The high frequency event in the vibration response observed in Figure 5(a) is associated with the rolling element exiting the defect.
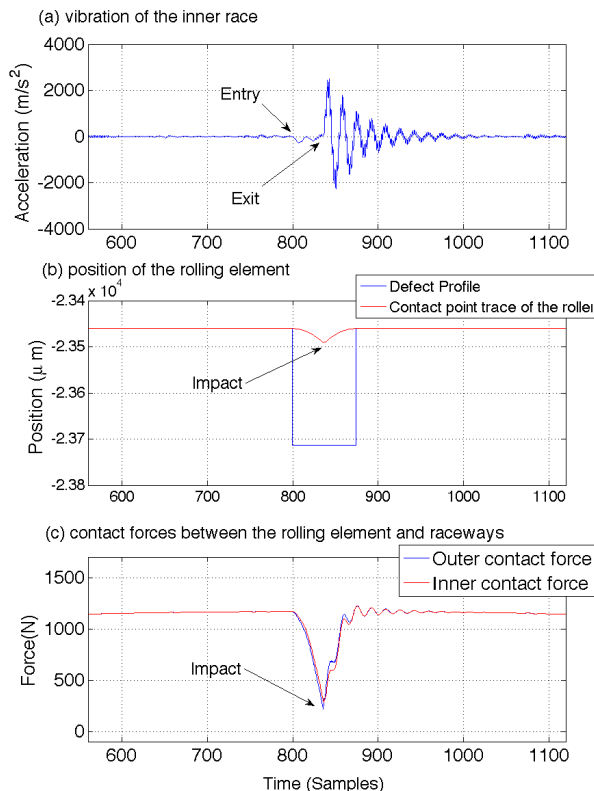

Figure 5: Simulated bearing with 1.1mm defect size. (a) vibration of the inner raceway. (b) position of the rolling element ($\rho_j + r_b$). (c) contact force between rolling element and raceways.

The low and high frequency events can also be explained by looking at the rolling element traces in Figure 5(b). The change of the acceleration at the entry is due to the trace of the rolling element following an arc path. As the centre of the rolling element reaches half way through the defect, the roll-

ing element hits the exit point of the defect. Consequently the rolling element has to suddenly change direction. This abrupt change in the direction of the movement causes a step change in the velocity and generates an impulse in the acceleration signal. In this example, the impact at the exit happens when the rolling element has travelled half way through the defect.

Figure 6 shows the experimentally measured acceleration of the test bearing conducted by Sawalhi and Randall (2011). They concluded that the entry to the defect exhibits low frequency content in the vibration signal and the impact happens when the centre of the rolling element has moved half way through the defect, which is consistent with the predictions of the proposed model described here.
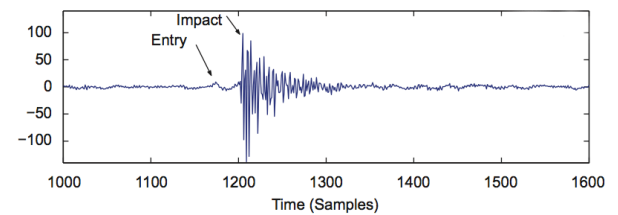

Figure 6: Experimental acceleration signal used for qualitative validation of developed model (Sawalhi and Randall, 2011)

The relative position of the two characteristic frequencies on the vibration signal is (Sawalhi and Randall, 2011)

$$l = \frac{T_i \pi f_r (D_p^2 - D_b^2)}{D_p f_s} \text{ (Samples)} \qquad (17)$$

where T_i is the time to impact in samples (measured from the start of the low frequency content in the vibration signal), f_r (Hz) is the rotational speed of the rotor and f_s (Hz) is the sampling frequency. Also, D_p and D_b are the pitch and rolling element diameters in mm, respectively. Sawalhi and Randall (2011) showed that the length of the defect can be estimated from the time between the occurrence of the low and high frequency events.

Equation (17) can be used to predict the defect length from the simulated signal in Figure 5(a). The number of samples between the entry and exit of the rolling element into the defect is T_i=23 in this figure. This gives an estimated size of the defect of $l = 1.11$ mm which matches the modelled length. Hence, the defect size estimation method proposed by Sawalhi and Randall (2011) works when the defect length is such that the rolling elements do not strike the bottom of the defect.

The presented simulations and the experimental observations by Sawalhi and Randall (2011) suggest that in bearings with a defect smaller than the diameter of the rolling element, the impact occurs midway through the defect. However, the modelled vibration response for a larger defect, which is considered in the next section, suggests that larger defects exhibit different characteristics.

Simulation of a large defect

In this section, the length of the outer raceway defect is increased in the simulations such that the rolling elements strike the bottom of the defect. The purpose of conducting these simulations is to highlight additional characteristics of the vibration response that cannot be predicted by previous models. The simulation results are studied in detail and the

vibration characteristics of a typical bearing with a large defect size are described.

The length of the bearing defect is chosen as 6.93 mm so that a rolling element loses contact with the outer and the inner raceway before hitting the defect at the exit point. The model can predict the impact of the rolling element at the bottom of the defect, which in turn generates high frequency excitation of the bearing that appears in the simulated vibration response. The simulation results of a bearing with 6.93 mm defect size are shown in Figure 7.
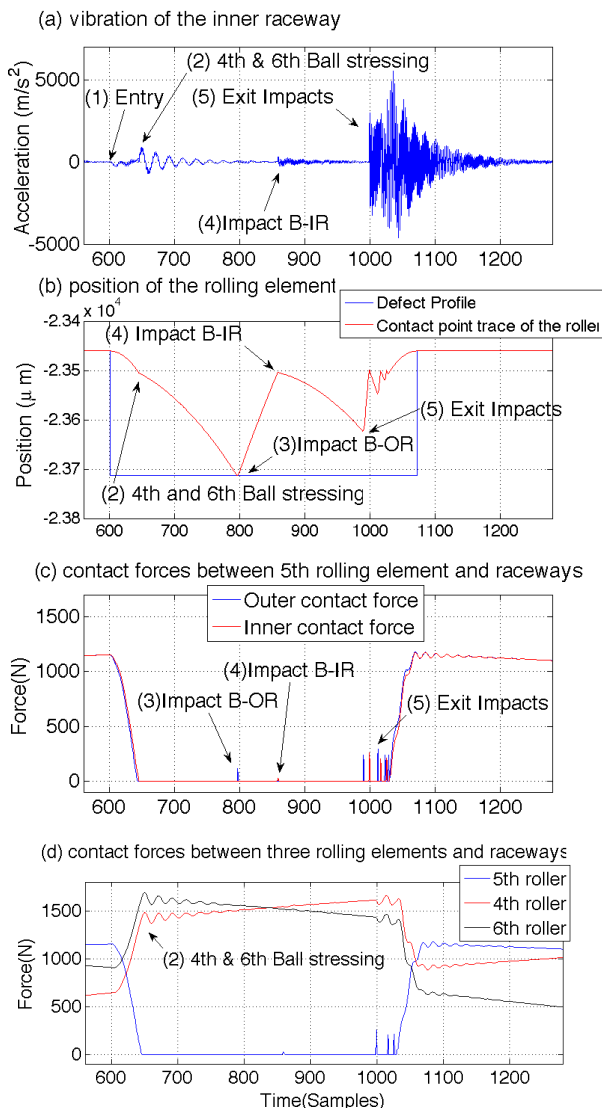

Figure 7: Simulation of large defect on the outer raceway (6.93 mm). (a) radial vibration. (b) trace of the 5th rolling element. (c) contact forces of rolling element-inner raceway and rolling element-outer raceway. (d) contact forces for the 4th, 5th and 6th rolling elements.

The key characteristics of the results are numbered on Figure 7 and are explained as follows:

1. **Rolling element entry:** the rolling element enters the defect and gradually de-stresses which causes a low frequency event in the vibration signal.

2. **Contribution of the 4th and 6th rolling element:** at this stage, the 5th rolling element completely loses contact with both raceways and the load has to be re-distributed among the other rolling elements. Figure 7(d) shows the

contact forces of the 4th, 5th and 6th rolling elements. At the time 1720 samples, there is an increase of load on the leading rolling element 6 and lagging rolling element 4, while the load is reduced on the 5th rolling element. The stressing and de-stressing of the 4th and 6th rolling elements introduces low frequency content in the vibration signal.

3. **Impact of the rolling element and outer raceway (B-OR):** after losing contact with the raceways, the rolling element travels through the defect and strikes the bottom of the outer raceway defect, as shown in Figure 7(b) at time 1870 samples. The contact time, which is the time from when the 5th rolling element contacts the bottom of the outer raceway to the time it first loses contact with the outer raceway, is shown in Figure 7(b) at 1870 to 1880 samples and is due to the damping introduced in the contacts. Figure 7(c) shows a half-sine contact force pulse of relatively low amplitude at time 1870 samples.

4. **Impact of the rolling element and inner raceway (B-IR):** the rolling element impacts the inner raceway before impacting the outer raceway at the exit point. This impact event generates high frequency signal content.

5. **Rolling element exit:** the rolling element re-stresses between the raceways which excites the high frequency resonance of the inner ring in this system. This re-stressing is followed by multiple impacts of the rolling element to the outer raceway and inner raceway at the exit.

CONCLUSION

This paper has presented a comprehensive nonlinear mathematical model that can predict the dynamics of defective rolling element bearings. The developed model has the capacity to model various bearing defect geometries.

The first simulation results of the proposed model are compared with experimental results and it is shown that the proposed model can predict the main characteristic events when a rolling element passes through the defect. These main characteristics are the low frequency event due to gradual de-stressing of the rolling elements at the entrance to the defect and the high frequency event due to the restressing at the exit of the defect.

A second simulation was conducted of a rolling element bearing with a larger defect in which the rolling elements temporarily lose contact with the raceways in the defect zone. The results of this case are studied and key characteristics of the vibration signal are discussed. The second simulation reveals the capability of the proposed model in predicting the impact events of a rolling element to the bottom of the fault that cannot be predicted by previous models.

Moreover, simulation of a larger defect revealed that the high frequency excitation of a bearing, with a defect size less than the diameter of the rolling element, does not necessary occur midway through the defect. Therefore, the simulation results of the proposed model can be used to develop and enhance bearing defect diagnostic algorithms.

Future work on this model and its applications could include further experimental validation and simulation of several different defect geometries on different components of a rolling element bearing.

ACKNOWLEDGMENT

References

Epps, I. & McCallion, H. 1994. An investigation into the characteristics of vibration excited by discrete faults in rolling element bearings. Annual Conference of the Vibration Association of New Zealand, Christchurch.

Harris, T. A. 2001. *Rolling bearing analysis*, Wiley.

Harsha, S. P. 2005. Nonlinear dynamic analysis of an unbalanced rotor supported by roller bearing. *Chaos, Solitons & Fractals,* 26**,** 47-66.

Harsha, S. P., Sandeep, K. & Prakash, R. 2003. The effect of speed of balanced rotor on nonlinear vibrations associated with ball bearings. *International Journal of Mechanical Sciences,* 45**,** 725-740.

Jang, G. & Jeong, S. W. 2004. Vibration analysis of a rotating system due to the effect of ball bearing waviness. *Journal of Sound and Vibration,* 269**,** 709-726.

Liew, A., Feng, N. & Hahn, E. 2002. Transient rotordynamic modeling of rolling element bearing systems. *Journal of Engineering for Gas Turbines and Power,* 124**,** 984-991.

Sawalhi, N. & Randall, R. 2008. Simulating gear and bearing interactions in the presence of faults: Part I. The combined gear bearing dynamic model and the simulation of localised bearing faults. *Mechanical Systems and Signal Processing,* 22**,** 1924-1951.

Sawalhi, N. & Randall, R. B. 2011. Vibration response of spalled rolling element bearings: Observations, simulations and signal processing techniques to track the spall size. *Mechanical Systems and Signal Processing,* 25**,** 846-870.

Sayles, R. & Poon, S. 1981. Surface topography and rolling element vibration. *Precision Engineering,* 3**,** 137-144.

Stachowiak, G. & Batchelor, A. W. 2011. Engineering tribology. Butterworth-Heinemann.

Sunnersjö, C. S. 1978. Varying compliance vibrations of rolling bearings. *Journal of Sound and Vibration,* 58**,** 363-373.

Tandon, N. & Choudhury, A. 1999. A review of vibration and acoustic measurement methods for the detection of defects in rolling element bearings. *Tribology International,* 32**,** 469-480.

Wardle, F. 1988. Vibration forces produced by waviness of the rolling surfaces of thrust loaded ball bearings Part 2: experimental validation. *Journal of Mechanical Engineering Science,* 202**,** 313-319.

Wijnant, Y. H., Wensing, J. A. & Nijen, G. C. 1999. The influence of lubrication on the dynamic behaviour of ball bearings. *Journal of Sound and Vibration,* 222**,** 579-596.